INFLUENCE OF ELEVATED TEMPERATURE ON PROPERTIES OF RADIATION SHIELDING CONCRETE WITH ELECTRIC ARC FURNACE SLAG AS COARSE AGGREGATE

A-L Beaucour[1*], P.Pliya[1], F. Faleschini[2], R. Njinwoua[1], C. Pellegrino[2], A. Noumowé[1]

[1] *University of Cergy-Pontoise, Laboratory of Mechanics and Materials of Civil Engineering (L2MGC), EA 4114, F-95000 Cergy-Pontoise, France*
[2] *Department of Civil, Environmental and Architectural Engineering, University of Padua, via Francesco Marzolo 9, Padova, Italy*

[*] *Corresponding author:*
email: anne-lise.beaucour@u-cergy.fr
phone: +33 (0)1 34 25 69 75

Abstract

The development of value-added materials from by-product of the steel-making process can promote sustainability in construction to move towards a circular economy. The use of Electric Arc Furnace (EAF) steel slag as heavyweight coarse aggregate to develop sustainable radiation shielding concrete could provide both technical and economic benefits with less environmental impact. This contribution investigates the behaviour at high temperature of a sustainable radiation shielding concrete. Thermal behaviour of EAF slag concrete was compared to another heavyweight concrete made of barite aggregates and to a normal-weight concrete. On one hand, the thermal stability of the three different aggregates was determined via simultaneous Thermogravimetry and Differential Scanning Calorimetry analyses and visual observations after 10°C/min heating. On the other hand, the evolution of thermal conductivity of concretes during heating, the residual mechanical properties and the assessment of potential spalling occurrence were investigated. Stereo-microscope and Scanning Electron Microscope pictures provide additional explanations by showing the paste-aggregate interface after heating at 450°C. The results indicated that EAF concrete displayed less strength reduction at increasing temperature. This improved behaviour is attributed to both the strong bond between the paste and the aggregates, and the better thermal behaviour of the EAF slag aggregates compared to barite aggregates.

Key words: Electric Arc Furnace slag ; Heavyweight concrete ; Barite aggregate ; Temperature ; Compressive strength; Dynamic modulus ; Recycle ; Thermal Conductivity

1. Introduction

Concrete is one of the most used materials to design shielding barriers for radiation protection. Among the typical structures that require an efficient and reliable shielding against radiations, there are reactor vessels, nuclear research facilities, hospitals and industrial facilities where high-current, low- and medium- energy proton accelerators are employed. Indeed, concrete has the ability to attenuate both gamma radiations, neutron radiations and mixed fields of both. Such property is acknowledged to the presence of heavyweight nuclei that are acting as a shield for gamma radiations, and due to relatively high content of water, that acts as a neutron-absorbing material (Kaplan, 1989).

Heavyweight concrete is a special type of concrete that finds large application to shield radiations, due to its improved attenuation capacity against gamma radiations. There are varying types of aggregates that can be used to achieve the desired increase in concrete density: barite, ferro-phosphorus, magnetite and hematite are the most well-known (Komarovskii, 1961; Mostofinejad et al. 1961; Ouda, 2015; Özen et al. 2015). Recently, a wide experimental research has been devoted to find sustainable alternatives to the above heavyweight aggregates, with both the aims to reduce the large economic and environmental costs caused by their use. Both negative and positive findings have been recorded. Çullu and Ertas (2016) have substituted lead mine waste to both limestone and barite aggregates in conventional and heavyweight concretes, respectively. They showed that lead mine waste aggregates do not absorb as much radiation as barite, but the absorbed radiation was higher than in the conventional concrete made with limestone. Alwaeli (2017) realized concrete specimens with scale and granulated lead–zinc slag waste as sand substitute, that displayed better attenuation capacity than convention concrete made with natural sand. Maslehuddin et al. (2013) and González-Ortega et al. (2014) performed preliminary experimental investigations about the radiation shielding properties of concretes with Electric Arc Furnace (EAF) slag. This by-product of steelmaking process represents a good candidate to cast heavyweight concretes with shielding properties, due to its high density and overall good mechanical strength. Such preliminary works highlighted the capability to produce heavyweight concretes EAF slag, with intermediate attenuation property between those of normal-mass and barite concretes. A recent work carried out by Pomaro et al. (2019) deals with a detailed experimental and numerical analysis on the mechanical and shielding properties of three kinds of concrete: a conventional one, made with normal-mass dolomitic aggregates; EAF slag concrete, including 100% of EAF slag as coarse aggregates substitution; and a barite aggregates concrete, as the heavyweight concrete of reference. Specimens were irradiated with

both a high-activity 60Co gamma-ray source (of 8.97TBq activity; dose rate of 53Gy/h at 20cm from the source) and a low-activity 60Co gamma-ray source (of 280kBq; dose rate of 6.24×10-7Gy/hour at 40cm from the source) to measure and compare the linear attenuation coefficients of each concrete mix. Then the results were also simulated via a Monte Carlo code assessing radiation transport through matter, to assess if the results are reliable. Results clearly highlight how the gamma-rays attenuation performance of EAF slag concrete is comparable to that of barite concrete; furthermore, its mechanical properties are noteworthy improved. Previous results on EAF concrete mechanical strength and durability-related performance in literature confirm this evidence (Arribas et al. 2015; Faleschini et al. 2017a, 2017b; Ortega-López et al. 2018; Papayianni and Anastasiou, 2010; Pellegrino et al. 2013), demonstrating how this by-product aggregate exhibit excellent properties.

This work represents a continuation of the above-cited work on EAF slag concrete, where one of the authors of this research was involved, aimed at studying in detail the thermo-mechanical properties of two heavyweight (made with EAF slag concrete and barite aggregates) and one normal-weight (made with dolomite aggregates) concretes. Indeed, there are many applications when shielding barriers might be exposed at the same time to radiation fields and high temperature, and in such strategic facilities, the guarantee of safe service life is of paramount importance. Some exemplary cases are those of the inner face of the shielding concrete in a nuclear facility, which is often exposed to direct heat from the reactor core, and that of spent nuclear fuel storage casks, that might be exposed for prolonged time at temperature up to 150°C.

While heating, the cementitious paste undergoes chemical and physical modifications mostly related to the departure of free and bound water of hardened cement paste. Moreover, thermal mismatch strain at the cement paste-aggregate interface can be at the origin of additional cracking (Xing et al. 2011). So, thermal exposure degrades physical properties like permeability or porosity and reduces mechanical properties like the elastic modulus or compressive and flexural strengths. Finally, the high compactness and low permeability required for these shielding elements can make heavyweight concretes more vulnerable to explosive spalling phenomenon. Spalling is the product of two concomitant processes: (a) thermo-mechanical process leading to expansion/shrinkage gradient and, (b) thermo-hydric process linked to water transfer in the pore network and leading to the build-up of pore pressure (Heap et al. 2013).

Only few studies have been carried out on high temperature behaviour of heavyweight concretes. The large majority of the studied concretes contained barite, magnetite or hematite aggregates.

Studies of Lo Monte and Gambarova (2014) have shown that barite concretes had favourable heat insulation properties thanks to their low thermal diffusivity compared to normal concretes. Residual compressive strength of barite concretes appeared to be slightly better than that of silico-calcareous concretes above 500°C (Lo Monte and Gambarova, 2014) but it was significantly lower than that of granite concrete (Ling and Poon, 2014). Ling and Poon (2014), and Horszczaruk et al. (2017) underlined the spalling sensitivity of barite concrete and the explosive spalling occurrence on the surface of the concrete specimens at low heating rate of 1°C/min and 4°C/min. This effect was attributed to barite aggregates low toughness and resistance to high temperatures, causing cracking when the aggregates are exposed to high temperatures. Horszczaruk et al. (2017) found that concrete with magnetite aggregates exhibited better residual mechanical properties in comparison to barite concretes; SEM images showed that no cracks were observed at 400°C in samples containing magnetite aggregate.

Gencel (2012) has shown that incorporating hematite into concrete leads to an improvement in its mechanical properties at an ambient temperature of 25°C. That is, after exposure to high temperatures, hematite concretes exhibited a higher overall compressive strength, flexural strength, splitting tensile strength, and elastic behaviour in comparison to the standard concrete with silico-calcareous aggregates. Gallé and Sercombe (2001) have shown a lower increase of the permeability of hematite high strength concretes between 250 and 400°C compared to silico-calcareous high strength concretes. To the author's knowledge, no spalling sensitivity tests were performed on heavyweight concretes with high heating rate. There are currently very limited researches with respect to the effect of high temperature on EAF slag concrete. Only Netinger et al. (2013) used steel slag as coarse aggregates; compared to dolomite aggregate. They observed that slag aggregate improved residual compressive strength up to 600°C, but beyond, residual mechanical performances of steel slag concretes underwent a more severe loss of performances. Liang et al. (2018), and Ducman and Mladenovic (2011) used steel slag as fine aggregate. According to Liang et al., residual properties of ultra high-performance concrete (UHPC) using steel slag as fine aggregate were significantly improved up to 1000°C compared to quartz powder, but Ducman and Mladenovic found lower residual strength at 800°C and 1000°C compared with refractory concrete made of bauxite aggregates. The worsen behaviour of slag concrete from 800°C could be explained by the mineralogical transformation of wustite into magnetite between 700°C and 800°C, this transformation being accompanied by volumetric expansion (Ducman and Mladenovic, 2011; Netinger et al. 2013).

Hence, in this paper an experimental research has been carried out to compare the thermo-mechanical behaviour of EAF slags aggregates concretes, barite concretes and normal-weight concrete.

The main aims of this work are to analyse the influence of EAF slag aggregates on the high temperature behaviour of concretes. Some tests are performed on aggregates and concretes with a heating rate of 10°C/min to assess the spalling occurrence. Otherwise, the evolution of physical and mechanical properties with temperature are investigated after heating/cooling at 1°C/min. The evolution of the thermal conductivity of concrete during the heating up to 600°C is also studied. The results that are presented give a comparison between the high temperature behaviour of EAF slag concretes and two other mixes, one heavyweight using barite aggregates and a normal-weight one made of dolomite aggregates. Furthermore, the study of the thermal stability of the three different aggregates and SEM observations provide some explanations on the concretes' behaviour depending on the type of aggregates.

2. Experimental program

2.1 Aggregates

Two different types of heavyweight coarse aggregates were used in the experiments: electric arc furnace steel slag aggregate (EAF) - coming from a steel making plant situated in Padova (Italy), where only carbon steel is produced - and a Barite aggregate (BAR), consisting of barium sulphate, coming from Italy too. Concerning the slag, during its productive chain, it was stabilised through an outdoor weathering process lasting for 3 months, then it was processed as an aggregate (i.e., it was sieved, crushed, subject to deferrization process, etc. until reaching the required grading), and lastly daily cycles of drying/wetting conditions were applied for a week on the final product. This process, currently adopted by many steelmaking plants in Spain and Italy, allows limiting further dimensional stability problems that might occur due to free CaO and free MgO expansion, and as well, it reduces the leaching of heavy metals in the concrete. Finally, normal-weight coarse aggregate (REF) composed of dolomite was used for the reference concrete. In all the mixtures, fine aggregate was an alluvial sand. The chemical composition of the raw materials was investigated using XRF analysis and shown in Table 1. The principal components of EAF slag, barite aggregates, coarse and fine natural aggregates are oxides of iron, lime and silica; barium oxide and sulphur trioxide; lime, magnesia and finally silica, respectively. The mineralogical composition of EAF was obtained by XRD analysis

using a Siemens D500 diffractometer with CuKα. The main mineral phases identified are wuestite (FeO), magnetite (Fe_3O_4), larnite (Ca_2SiO_4) and gehlenite ($Ca_2Al_2SiO_7$) and calcite ($CaCO_3$). This latter probably comes from the hydration then the carbonation of CaO during the weathering stage.

Coarse natural aggregates and EAF aggregates were provided into various fractions of size 4-16 mm while for barite aggregate, the size was between 4-14 mm as shown in Table 2, which presents the physical properties of the aggregates. EAF slag coarse aggregate and barite aggregate have high and close specific gravities, 3.85 and 3.82, respectively, while natural coarse aggregate has a specific gravity of 2.7. Besides, the water absorption - influencing the water content and therefore the concrete's high temperature features - of barite aggregate, EAF slag coarse aggregate and natural coarse aggregate was 1.90%, 0.84% and 0.75%, respectively. A Water Reducing Admixtures was used to adjust the workability of the concrete mixes.

Table 1. Chemical composition of the aggregates by XRF analysis (Pomaro et al. 2019)

	Dolomite (%)	**Barite (%)**	**EAF slag (%)**	**Fine NA (%)**
CaO	55.74	-	30.30	19.01
SiO_2	4.31	5.01	14.56	53.77
MgO	39.94	-	2.97	10.32
BaO	-	59.86	-	-
SO_3	-	35.14	-	-
Fe_xO_y	-	-	33.28	3.19
Al_2O_3	-	-	10.20	11.90
MnO	-	-	4.34	-
Cr_2O3	-	-	2.67	-
K_2O	-	-	-	1.81

Table 2. Physical properties of aggregates

	Dolomite (REF)	**Barite (BAR)**	**Slag (EAF)**	**Fine NA**
Size (mm)	4-16	4-14	4-16	0-4
Apparent density (EN1097-6) (kg/m^3)	2701	3817	3854	2703
Water absorption (EN 1097-6) (wt.%)	0.75	1.90	0.84	1.18
Water porosity (EN 1097-6) (%)	2.03	7.25	3.24	3.19
Los Angeles coefficient (EN 1097-2) (%)	28	65	15	/
Origin	Alluvial	Crushed	Crushed	Alluvial

2.2 Mix design

Concrete mixtures were prepared using cement CEMI 52.5R. All the mixes contain 400 kg/m^3 of cement with a water/cement (w/c) ratio of 0.4, which is the recommended ratio when it comes to concrete that are to use for nuclear purposes (Topcu, 2003). Detail of mix design used for concrete is presented in Table 3. The water reducing admixture is added in order to have a slump ranging from 150 to 210 mm, therefore corresponding to class S4, according to the standard NF EN 206-1. The ratio (w/c) and the total volume of aggregate were the same for the different mixes. However, the amount of water reducing admixture was different for each mix design to obtain the required class S4.

Table 3. Mix proportions for one m^3 of the investigated concretes

Components (kg/m^3)	**REF-concrete**	**BAR-concrete**	**EAF-concrete**
Cement	400	400	400
Silico-calcareous aggregate	971	-	-
Barite aggregate	-	1371	-
EAF slag aggregate	-	-	1270
Alluvial sand	913	897	966
Water Reducing Admixtures (dry extract)	3.2	4.0	3.2
Slump (mm)	190	150	210
Fresh Density (kg/m^3)	2412	2810	2771

2.3 Specimens preparation

For each type of mixture, eighteen cylindrical specimens of 100 mm x 200 mm (diameter x height) were cast. The concrete specimens were cured in sealed bags with a damp cloth to maintain a humidity-saturated atmosphere for a period of about three months. The moisture content was determined for each concrete mix design on 4 – 6 (200g - 400g) concrete's pieces coming from 100 mm x 200 mm cylindrical specimens broken after the compression test. The average moisture by mass of each mix design, before tests, were 4.6%, 4.0% and 4.1% for REF, BAR and EAF concretes, respectively. The lowest density of its solid phase compared to BAR and EAF concretes explains the highest value for REF concrete. These values in weight percent correspond to volume fraction of 11.0 % ± 0.3%, 11.2% ± 0.4% and 11.4% ± 0.2% for REF, BAR and EAF concretes, respectively. The average water amount being approximately the same, there is therefore a valuable basis for the comparison of the different concretes test results

after being heated. After 90 days of curing, one of the 100 mm x 200 mm cylindrical specimens for each mix design was cut into 4 slices of 40 mm thickness. Two slices for each mix design were pre-dried in an oven at 80°C before the thermal conductivity test and the two others were kept in sealed plastic bags with a damp cloth for heating-cooling tests. Two concrete cylinders for each mix design were cut before heating in two 100 x 100 mm cylinders. They were intended for wave velocity measurements before and after heating.

2.4 Heating and cooling methodology

In order to study the high temperature behaviour of the concrete mixes, two different heating rates have been applied for the heating tests. On the one hand, to study the "spalling" sensitivity, a heating rate of 10°C/min was used, and on the other hand, to investigate the concretes' residual properties (physical and thermomechanical one) as a function of temperature a slow heating rate of 1°C/min was performed. An electric furnace with inner dimensions 1300 x 1010 x 1040 mm (L x D x H) with a power of 150 KW was used (Figure 1). Temperature rise was controlled by a regulator-controller connected to a thermocouple in the furnace. Type K thermocouples, connected to an automatic data acquisition were used to monitor temperatures, every 30 seconds in the furnace, positioned on specimens' surface. The surface temperature of concretes controls the temperature rise of the furnace. To evaluate the spalling sensitivity, some aggregates and 100 mm x 200 mm concrete specimens were heated up to 600°C from room temperature (at a rate of 10°C/ min) with a 2hours stabilization at 600°C and a cooling rate of -1°C/min to room temperature. The heating rate of 10°C/min has been chosen because the risk of spalling is higher at moderate heating rate than at faster heating rate (Mindeguia et al. 2013; Bangi et al. 2012; Yermak et al. 2017). As higher rate of heating induces high thermal gradient, a large number of surface cracks occurs. These cracks allow significant amount of vapour and liquid water to be drained out from the specimen that limit the risk of spalling.

In order to study residual properties, concretes were subjected to different heating-cooling cycles of 150, 300 and 450°C at a heating rate of 1°C/min from the room temperature, with a 2 hours stabilization at the target temperature and a cooling rate of -1°C/min to room temperature. The low heating rate ensures the homogeneity of temperature and limits the thermal gradient within the specimen (Rilem, 1995).

a) b) c)

Figure 1: Heating cooling device: a) Furnace b) temperature recording system c) concrete specimens inside the electric furnace

2.5 Testing procedure

The evolution of the concrete microstructure with temperature was studied analysing concrete porosity, and with Scanning Electron Microscopy (SEM) observations. Residual properties such as the compressive strength (f_c) and the dynamic Young modulus (E_c) were measured after different heating-cooling cycles at 1°C/min. Thermo-physical properties like conductivity and specific heat were investigated as a function of the temperature.

2.5.1 Residual tests

Dynamic modulus (E_c) was measured on 100 mm x 100 mm cylindrical specimens at room temperature and after heating-cooling at 150°C and 300°C (1°/min) with a Pundit lab instrument (Figure 2), evaluating the ultrasonic pulse velocity (*UPV*), according to European standard EN 12504-4. The device sends an electrical signal into the sample. This signal is transformed into longitudinal waves by a piezoelectric transducer. The waves propagate in the sample from one transducer to the other (at a distance *L*) and are reflected back to the starting transducer. The apparatus measures the time "*t*" between two successive echoes, from which the velocity "*v*" of the longitudinal ultrasonic waves is calculated. The dynamic modulus of elasticity is determined from P-wave velocity and concrete density thanks to Eq. 1:

$$E_c = \frac{v^2 \cdot (\rho + \rho\upsilon) \cdot (\rho - 2\rho\upsilon)}{1 - \upsilon} \quad (1)$$

With E_c the dynamic modulus, v the velocity of the ultrasonic waves, ρ the density of the concrete at the studied temperature, and v the Poisson ratio (v = 0.2 for the concrete).

Figure 2: Ultrasonic pulse velocity apparatus for the assessment of the dynamic elastic modulus

Compressive strength (f_c) was measured on three 100 mm x 200 mm cylinders for each mix after heating-cooling at 150°C and 300°C at 1°C/min and also at 600°C after spalling sensitivity tests at 10°C/min. Concrete specimens were tested under uniaxial compressive loading on an INSTRON 3000 kN hydraulic press, with imposed stress rate of 0.5 MPa/s according to EN 12390-3 (2019).

Concrete mass loss was obtained on three cylindrical specimens 100 mm × 200 mm for each temperature level and for each concrete mix design. Specimens were weighted before and after each heating-cooling cycle in order to determine the total mass loss during the heating-cooling protocol.

Water-porosity (P) was measured on three concrete pieces (200 g average weight), for each concrete mix and for each target temperature. Before the test, samples were dried at 80°C until achieving a constant mass. The method, according to the standard NF P18-459, requires to saturate the sample with deionized water by using the capillary rise methodology. For this purpose, the oven-dried samples were placed in vacuum to evacuate air from the internal pores. This procedure should be carried out for 48h. After the complete saturation of the sample, the amount of water should be evaluated by the gravimetric method. The weighting is carried out immediately after disconnecting the vacuum-pump. The gravimetric water content, obtained by the relation between the saturated weight and the dried weight (48h in an oven), should be multiplied by the bulk density (g/cm^3) to measure the volumetric water content. Eq. 2 gives porosity P, expressed as the percentage volume:

$$P = \frac{(m_{sat} - m_{dry})}{m_{sat} - m_{sat\_im}} \cdot \rho_w \cdot 100 \qquad (2)$$

Where m_{sat} represents the weight of saturated surface dry sample in (g), m_{dry} the weight of dry sample in (g), m_{sat_im} the weight of the immersed saturated sample in (g) and ρ_w the water density in (g/cm^3). After removing the sample from water, it is quickly and carefully wiped to remove the superficial water, and then placed on the hydrostatic balance and massed completely immersed to obtain the above measures.

Concrete slices of 40 mm x 100 mm were used for carrying out visual inspection with a stereo-microscope, and microstructural analysis was performed via a scanning electron microscope ZEISS Gemini SEM 300. Samples were dried, polished, immersed in the resin under vacuum after cooling and then coated with nickel.

2.5.2 Thermal properties during heating

Thermal properties of the different concretes such as thermal conductivity and specific heat were assessed. Besides, TGA/DSC tests have been realised on the different types of aggregates.

Thermal conductivity (λ) was measured during heating with the Hot Disk probe TPS1500. The system is based on the technology of the Transient Plane Source (TPS). This method has been developed at Chalmers University of Technology by Gustafsson et al. (Gustavsson et al. 1994). A mica probe with radius 14.610 mm, consisting of a very fine nickel double spiral (thickness 10 µm) covered with two thin layers of electrically-insulating material, is placed between two concrete cylinders (100 mm x 40 mm: diameter x thickness). The probe sends an electric current which raises the temperature of the specimen. The result is recorded with the increasing of resistance. Each concrete cylinder must have a flat surface to avoid contact defects with the sensor. Concrete cylinders were pre-dried at 80 °C until a constant mass was obtained before the measurement. The test was carried out at room temperature conditions, then increasing temperature from 20°C to 600°C in a 5 L electric furnace controlled by the Hot Disk Software. The heating rate was 1°C/min and the maximum temperature achieved was 600°C. For each target temperature, four measurements were taken under isothermal conditions.

Thermogravimetric analysis / Differential Scanning Calorimetry analysis (TGA/DSC) tests were carried out under vacuum in nitrogen gas. TGA/DSC tests give the mass change of a sample during heating and compare the evolution of its thermal properties to that of a Al_2O_3 reference sample. The difference in temperature is measured and could be converted into a heat flow difference with an appropriate calibration. For each type, a representative aggregate

sample was dried at 80°C to constant mass and then ground into a fine powder using an automatic disk vibrator type RS200 from Retsch. Aggregate samples are then kept in sealed plastic bags until the thermal analysis test was performed with a NETZCH STA 449 F1 Jupiter device. A 60 mg weight is placed on the thermo-nanobalance of the apparatus and weighed accurately (± 0.025 µg) throughout the test. The heating rate is 10°C/min up to 1000°C.

3 Results and discussion

This section presents, first, the results obtained on the thermal behaviour of aggregates, and then thermal properties and residual behaviour of concretes made with the studied aggregates.

3.1 High temperature behaviour of aggregates

3.1.1 Thermal analysis (TGA/DSC)

Figure 3 presents TGA/DSC curves for dolomitic alluvial aggregate (REF). The total mass loss is about 16%. Two stages of weight loss can be appreciated: 2% mass loss between 400°C and 500°C, and 14% mass loss in the range of 600 and 800°C. The decomposition of dolomite $CaMg(CO_3)_2$ between 600 and 800 °C is pointed out with two endothermic peaks (735°C and 775-800°C) due to the double decarboxylation of dolomite (Eqs. 3-4).

$$CaMg(CO_3)_2 \rightarrow CaCO_3 + MgO + CO_2 \quad (3)$$

$$CaCO_3 \rightarrow CaO + CO_2 \quad (4)$$

The other peak observed within the range 775-800°C can be related to calcite decomposition.

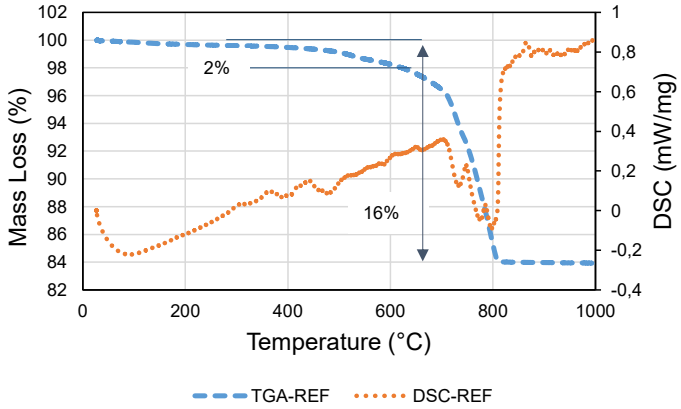

342 *Figure 3: TGA and DSC curves for alluvial dolomite aggregate (REF)*

343

344 Figure 4 presents TGA/DSC curves for BAR and EAF aggregates. The loss of weight for BAR
345 is very low with a value of 0.38%. It mainly occurs before 300°C and after 900°C. Concerning
346 EAF slag, the total weight loss is 0.52%. A weight loss of 0.1% can be observed in the
347 temperature range from 600°C to 700°C that can be attributed to calcium carbonate
348 decomposition as calcite was identified by XRD analysis. Finally, a slight weight gain is visible
349 between 800°C and 950°C, which is possibly linked to the oxidation of some iron-based
350 compounds present in the slag, in agreement with Galán-Arboledas et al. (2017) and Shih et al.
351 (2004). An endothermic peak occurs at 573°C in DSC curve of EAF aggregate that correspond
352 to the α-β transformation of quartz.

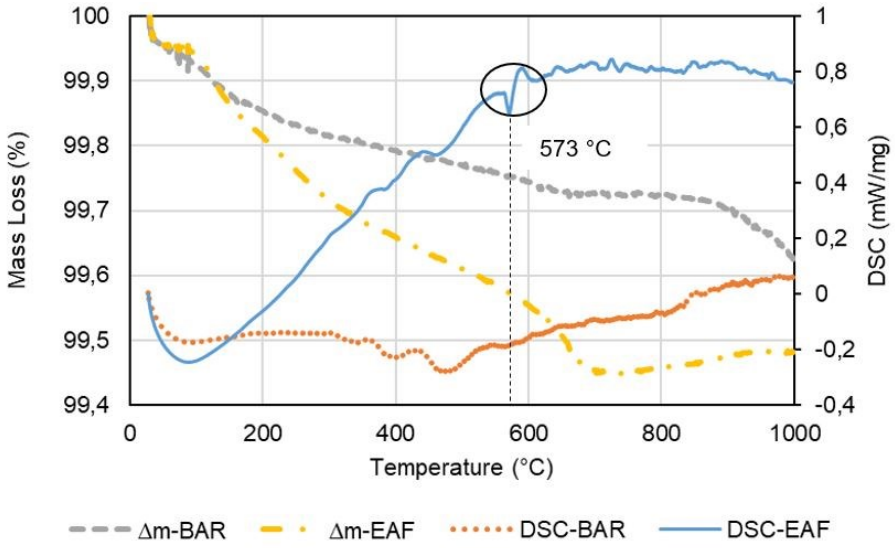

353

354 *Figure 4: TGA and DSC curves for BAR and EAF aggregates*

355

356 **3.1.2 Visual observations on heated aggregates**

357 In order to investigate the influence of the initial moisture content, aggregates were tested either
358 in saturated or in their natural moisture state, at room temperature. In saturated conditions,
359 aggregates were immersed in water from two to three days. Figure 5 shows the aggregates

before and after the heating test at 600°C with a rate of 10°C/min under saturated and non-saturated conditions.

For REF aggregate, both for the saturated or unsaturated aggregates, there was no spalling after the heating test and only few cracks were observed. Nevertheless, after the heating test, when kept at room temperature, REF aggregate showed some cracks whose length increased. This could be the result of the rehydration of CaO or MgO with ambient moisture, as the TGA/DSC curve shows the beginning of dolomite decomposition at 600°C.

BAR aggregates, that had been saturated before heating, spalled entirely and came into a powder form. While, in unsaturated conditions, only part of the aggregates spalled. Smaller spalled pieces could be related to higher released energy due to the build-up of high pore pressure. Works of previous authors pointed out that barite micro-fractured structure brings in intersecting surfaces that act as preferential paths in favouring the splitting of the rock particle (Witte and Backstrom, 1954). This brittle mechanical behaviour may be promoted by the barite's thermal instability. Furthermore, the high porosity of barite aggregates leads to a higher water content that is an important parameter promoting the explosive spalling risk. As shown further on SEM images (Fig. 8), closed rounded micro-porosity is observed within barite aggregates and might be fluid-filled (Valenza et al. 2000). The increase of internal pressure in those closed micro-pores during heating could also contribute to the aggregate's splitting.

For EAF aggregates, either in saturated or unsaturated conditions, no explosive spalling occurred.

Figure 5: Comparison of the three different types of aggregates before and after the heating test at 600°C (10°C/min) under saturated and unsaturated state before heating

3.2 High temperature behaviour of concretes

3.2.1 Analysis of the damage of concretes

3.2.1.1. Visual observations after different heating rates

No explosive spalling phenomenon was observed after 1°C/min and 10 °C/min heating tests. Nevertheless, one third of the EAF and BAR tested concrete cylinders exhibited some "aggregate spalling".

Table 4 gives a summary of the moisture content of specimens before heating and the number of concrete specimens damaged after heating test. Concretes with natural aggregates (REF) did

not exhibit any spalling phenomena during heating, whatever the moisture content (3.8%–4.8%), but some cracks occurred. Instead, concretes with barite aggregates (BAR) and EAF slag showed some surface spalling (Fig. 6). For these concretes, the spalling depth was about 5 mm. The aggregate spalling phenomenon observed on both concretes was more important for the heating test at 450°C with 1°C/min rate than for the spalling sensitivity test at 10°C/min. These crater-shaped spalling can be attributed to aggregate failures or high thermal expansion of coarse aggregates near the specimen surface. This evidence can be related to results on aggregates heating tests which have highlighted the thermal instability of barite aggregate. Ling and Poon (2014) also showed that spalling occurred on the surface of barite concrete samples, after exposure to 600°C at 5°C/min. The spalled pieces of concrete are located above aggregate particle. The authors explain it by the high thermal expansion of barite aggregate. The thermal expansion coefficient of barite aggregates according to Witte and Backstom (1954) is 20.6 $x10^{-6}.K^{-1}$. No difference in spalling behaviour could be correlated with the different water moisture values before heating (Table 4).

Table 4: Summary of concrete damage after heating test (at 600°C with 10°C/min) and moisture content of specimens before heating

Concretes	Degradation type			Moisture content before heating	
	Aggregate Spalling *	Ratio of impacted Specimens	Maximum depth of aggregate spalling	(% weight)	(% volume)
BAR	+	1/3	5mm	4.0 ± 0.4	11.2 ± 0.4
REF	-	0/3	-	4.6 ± 0.3	11.0 ± 0.3
EAF	+	1/3	5mm	4.1 ± 0.2	11.4 ± 0.2

*: +: observed degradation, - : No degradation.

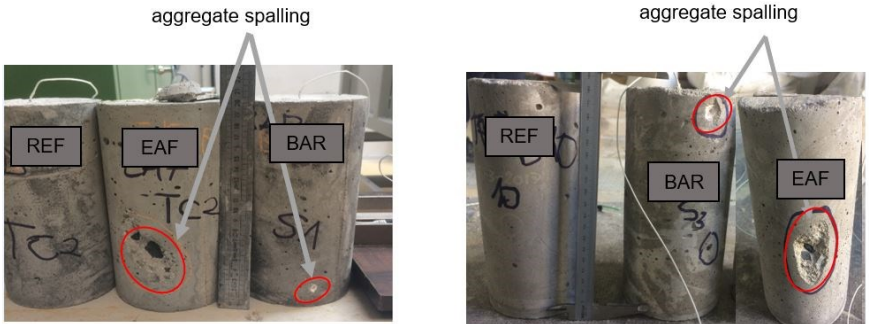

a) b)

Figure 6: Illustration of the "aggregate spalling" phenomenon on BAR and EAF concrete specimen of 100 mm x 200 mm dimension: a) after 10°C/min heating test up to 600°C; b) after slow heating test at 1°C/min up to 450 °C

3.2.1.2. Microscopic observations after heating at 1°C/min

In order to compare and analyse the evolution of cracking with temperature in each concrete series, 100 mm x 50 mm slices sawn from 100 mm x 200 mm concrete cylinders were submitted to heating-cooling at 1°C/min up to 150°C, 300°C and 450°C. Regardless of the type of concrete tested, after heating to 150°C no visible damage was detected under the stereo microscope. After 300°C test, some cracks mainly located within the cement paste were observed under the stereo microscope. The colour of some dolomite particles has turned into red at 300°C. Figure 7 shows pictures of REF, BAR and EAF concretes after heating-cooling cycle at 450°C taken with stereo-microscope and scanning electron microscope (SEM).

For the REF concretes, reddish spots have been observed after heating at 450°C, likewise, a radially propagation of cracks within the matrix surrounding the aggregate was noticed, as well as some tangential cracks at the paste-aggregate interface. On one side, reddish spots could be easily linked to the presence of iron oxides inside the alluvial sand, that would turn into a reddish-brown coloration at increasing temperature. On the other side, color-change of some dolomitic grains into red was already reported by other authors, i.e. by Hager et al (2016). SEM observations highlighted the presence of an aggregate removed from the cement paste. Cracks reveal a thermal mismatch between the aggregate and the cement paste and confirm the low strength interface due to smooth rounded aggregate.

For BAR concretes, no cracks were observed at the paste-aggregate interface, showing a good adhesion between paste and aggregate. Some cracks crossing through the barite aggregate have

occurred. Backscatter electron images show many micro-pores with a rounded shape within the barite aggregate (Fig. 8). Fluids may be trapped within these vacuoles due to the hydrothermal origin of the barite itself. According to several authors, aqueous and hydrocarbons fluid inclusions occur within barite, with variable liquid to vapour ratios (Thomson et al. 1992; Ulrich et al. 1988). During heating, internal pressure increases and might initiate the fracturing process of the inclusion walls. Some micro cracks were observed in the paste of the EAF concretes, no crack appeared at the paste-aggregate interface. Cracks observed in the surrounding cement matrix do not seem linked to the EAF aggregate. This confirms a good bond between EAF particles and cement paste.

Type	(Optical) Microscopic observations	Scanning electron microscopy
EAF	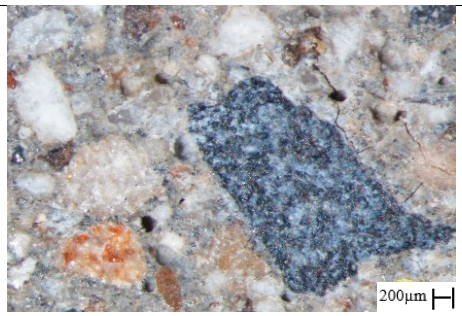	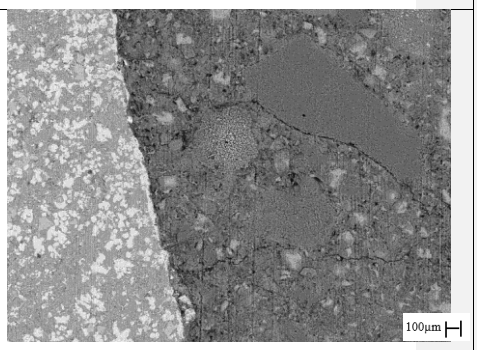
BAR		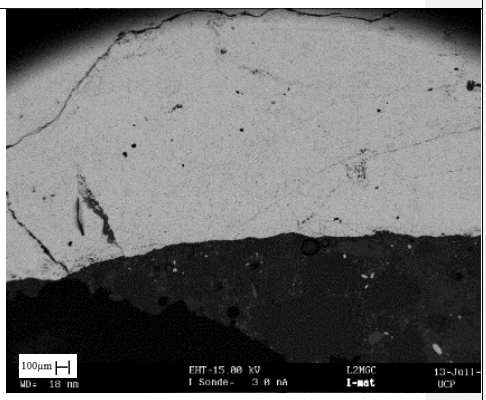
REF	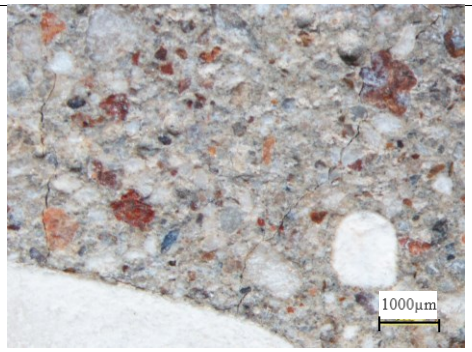	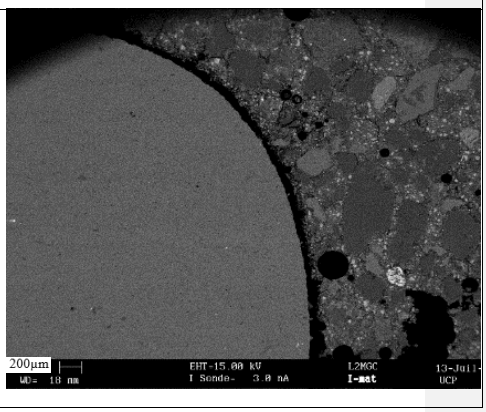

447

448 *Figure 7: Stereo-microscope and Scanning Electron Microscope (SEM) observations of*
449 *concretes after heating-cooling at 1°C/min up to 450°C*

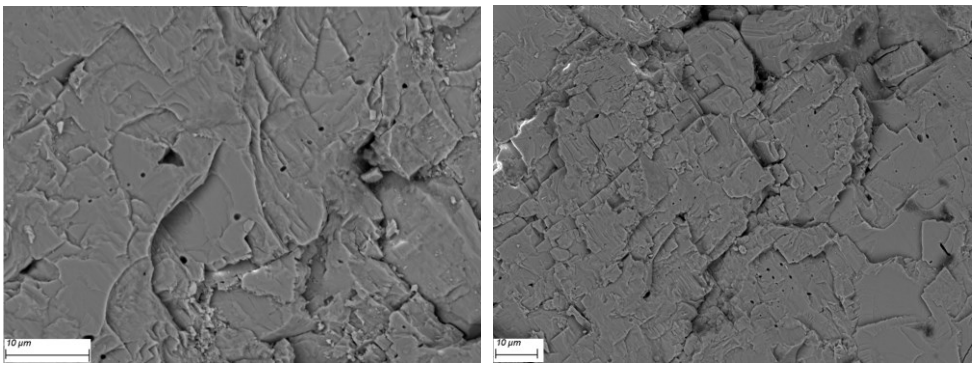

Figure 8: SEM micrographs of barite aggregates after heating-cooling at 1°C/min up to 450°C

3.2.2. Residual physical properties

Residual physical properties were measured after heating-cooling at 1°C/min. Indeed, to assess the evolution of the material properties in function of the temperature, the heating/cooling rate should be sufficiently low to ensure a homogeneous temperature distribution within the sample.

3.2.2.1 Mass loss

Figure 9 shows the evolution of REF, BAR and EAF concretes mass loss as a function of temperature. The standard deviation ranges from 2 to 10 g. Because of the difference in concrete density, the mass loss was not evaluated in percentage, but by difference of masses, to allow a direct comparison between the three series of concrete. Only not spalled specimens were taken into account in the calculations.

As expected, the mass loss increases with temperature. At 150°C, BAR concrete exhibits a slightly higher loss as compared to EAF and REF mixes. This may be attributed to the higher water absorption capacity of BAR aggregate (Table 2). From 300 to 450°C, the three concretes show a similar mass loss trend. Most of the loss occurs before 300°C due to the evaporation of capillary water from macro-pores, evaporation of gel water from gel pores of cement paste and partial dehydration of C-S-H (Zhang 2011). The mass loss observed at 450°C may be due to portlandite decomposition.

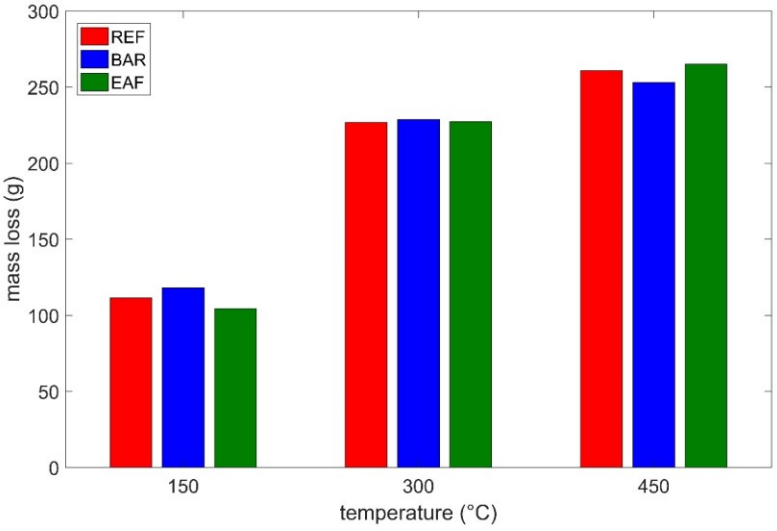

Figure 9: Mass loss of 100 mm x 200 mm concrete cylinders concretes

3.2.2.2 Density and porosity

At 20°C, EAF concretes naturally lead with an average density of 2805 ± 39 kg/m^3 because of the high density of their aggregates. The BAR concrete comes in second place with a density of 2766 ± 35 kg/m^3, a value quite close to that of EAF mixture. The REF concrete is a normal-weight concrete with 2401 ± 9 kg/m^3. Figure 10 shows the evolution of density with heating temperature for the different concretes, both in (a) absolute and (b) percentage terms. As expected, the concrete density decreases with temperature. Until 300°C, both densities of EAF and BAR are around 2600 kg/m^3 that is acknowledged as the unit mass volume threshold for a heavyweight concrete. At 450°C, the density of the concretes was 2500 kg/m^3.

Figure 11 shows the evolution of the residual porosity with the heating temperature for REF, BAR and EAF concretes. After 150°C heating-cooling test, the residual porosity of REF, BAR and EAF concretes were 13.0%, 14.5 % and 13.2%, respectively. The residual porosity of all concretes tested increases with temperature. Barite concrete has the highest values of residual porosity compared to that of the REF and EAF concretes. This is consistent with the higher porosity value of barite aggregate (Table 2). The REF and EAF concretes show a higher increase of porosity than BAR concrete between 300 and 450°C.

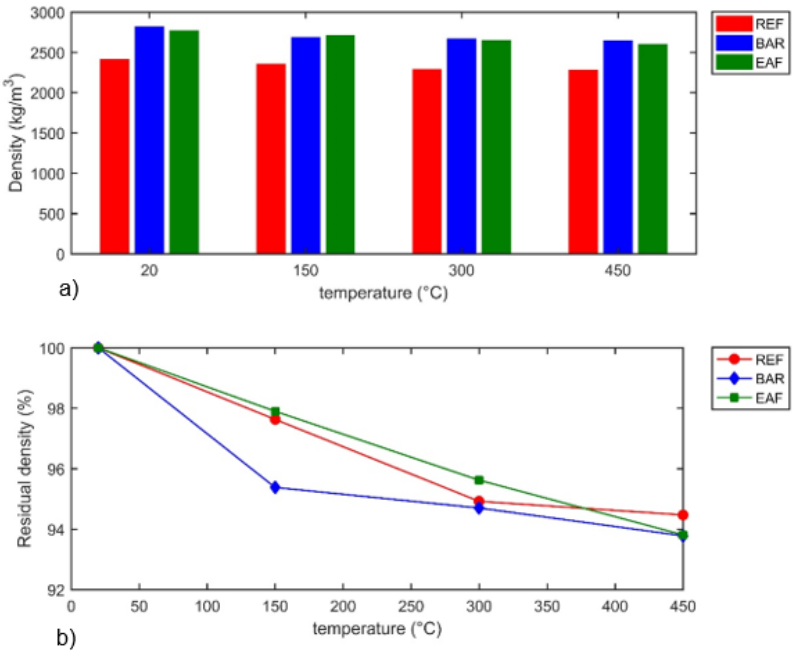

492

493 *Figure 10: Residual density as a function of the heating temperature*

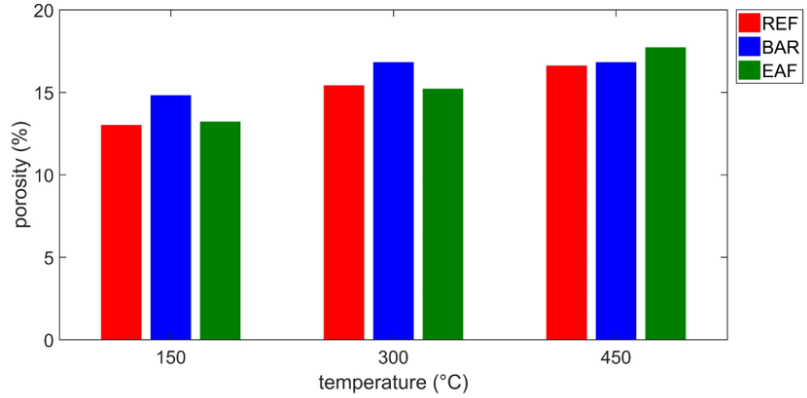

494

495

496 *Figure 11: Residual porosity as a function of the heating temperature*

497

3.2.2.3 Residual mechanical properties of concrete

Mechanical tests performed on the heated specimen after cooling allowed to evaluate the effect of the aggregates on mechanical strength after exposure to high temperatures. Table 5 gives the mechanical properties of the different concretes at room temperature after 90 days. The EAF concrete has the highest strength as well as the highest dynamic modulus (E_c), as compared to BAR and REF concretes. Hence, EAF concrete exhibits enhanced mechanical properties compared to the other mixtures, in terms of compressive and dynamic modulus. Such improved behaviour can be attributed to several reasons: relatively high compressive strength of EAF slag (higher than 130 MPa (Manso et al. 2004)); crushed shape, which is found to improve the adherence with the cementitious matrix (Abu-Eishah et al. 2012); reduced thickness of the interfacial transition zone (ITZ), due a combined physical-chemical interaction between slag and cement paste (Chan et al. 1996; Maslehuddin 2003) that results in a less porous and cracked ITZ. Indeed, it has been demonstrated that the surface of EAF slag enriches in calcite due to the hydroxylation of free CaO that is present in low amount in the slag, favouring the bond with cement paste.

Figure 12 shows the evolution of residual compressive strength of REF, BAR and EAF concretes from room temperature to 450 °C. As expected, exposure to elevated temperature leads to a reduction in the residual compressive strength of concrete specimens. Overall, the residual compressive strength values of EAF concretes were higher than those of REF and BAR concretes, whatever the exposure temperature.

Between 150 and 300°C, the residual relative compressive strength of the REF concrete is almost constant, while there is a residual strength decrease for the heavyweight concretes (Figure 12(b)). However, between 300 and 450 °C, the relative residual strength loss of the REF concrete (50%) is higher compared to that of EAF (3%) and BAR (12%) concretes. At 450°C, REF concrete only keeps 20% (9.0 MPa) of its initial compressive strength while EAF and BAR concretes exhibit 60% (39 MPa) and 53% (25 MPa) of their initial strength, respectively. After the residual compressive strength test, the failure surface of REF concretes heated at 450°C shows that aggregate particles had been debonded from the paste. Indeed, dolomite aggregate particles are rounded and smooth surface textured; this fact explains a lower bond strength than that developed between cement paste and angular aggregate particles with rough texture, like EAF or BAR aggregates. The higher increase in porosity of REF concrete between 300°C and 450°C might be due to micro-cracks occurrence at the paste aggregate interface.

At room temperature, as for compressive strength, EAF concretes have a higher dynamic modulus (Figure 13(a)) compared to BAR and REF concretes ones. However, the relative modulus decrease with temperature is similar for the two heavy-weight concretes, EAF and BAR concretes.

Table 5: Mechanical properties of the different concretes at 90 days

Concrete	Hardened density (kg/m^3)	$f_{c,90days}$ (MPa)	E_c (GPa)
REF	2401.0 ± 8.7	49.2 ± 2.2	48.2 ± 2.2
BAR	2765.7 ± 35.1	46.5 ± 7.0	37.5 ± 1.1
EAF	2804.1 ± 39.3	65.4 ± 2.4	56.3 ± 3.0

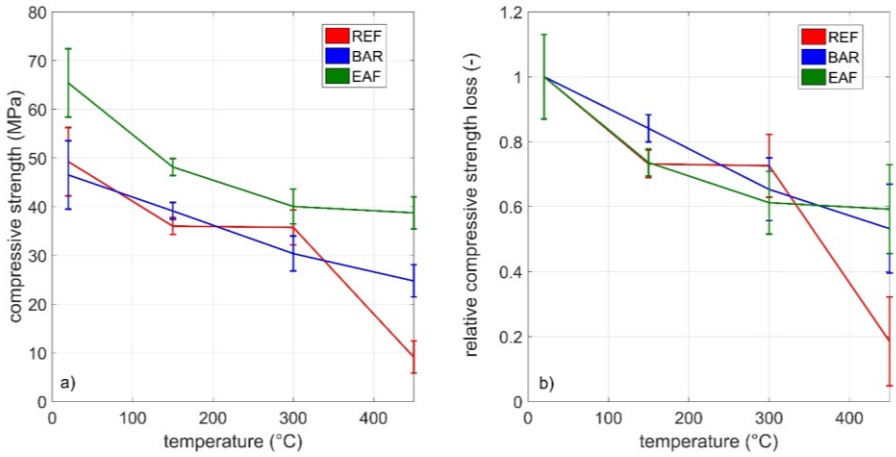

Figure 12: Residual compressive strength (a) and relative residual compressive strength (b) as a function of the temperature

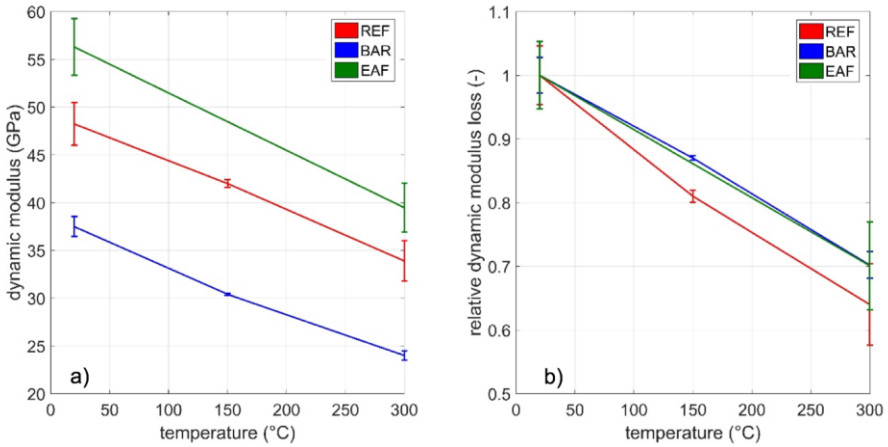

Figure 13: Residual dynamic modulus (a) and relative residual dynamic modulus (b) as a function of the temperature

3.2.3 Evolution of thermal conductivity during heating

Table 6 lists the thermal properties of REF, BAR and EAF concretes at room temperature. As aggregates occupy a large volume in concrete, the heat transfer of concrete depends mainly on the aggregate composition. So, concrete thermal conductivity is mostly affected by mineralogical composition of aggregates, and by porosity value, due to the low thermal conductivity of air, being 0.026 $W.m^{-1}.K^{-1}$. The thermal conductivity of heavyweight concretes is 1.34 and 1.51 $W.m^{-1}.K^{-1}$ for BAR and EAF concretes, respectively, being lower than that of concrete made with dolomite aggregates, which is 2.05 $W.m^{-1}.K^{-1}$. BAR concrete exhibits a higher porosity (Figure 11) related to the higher porosity of barite aggregate (Table 2). This high porosity may partly explain the low thermal conductivity value of BAR concrete. Very few data are available in literature about thermal conductivity of barite concrete: Glinicki et al. (2015) had measured a thermal conductivity value of 1.35 $W.m^{-1}.K^{-1}$ for a barite aggregate concrete of 2776 kg/m^3 density.

About EAF, Adegoloye et al. (2015) had already reported 20 to 24% lower thermal conductivity of EAF slag concrete compared to concrete containing silico-calcareous aggregate. Some EAF slag particles may have a vacuolar porosity that might explain the lower conductivity value. The barite aggregate concrete exhibits a specific heat much lower than that of the two other concretes, whose specific heat are quite close. The thermal diffusivity is defined as:

$$a = \lambda/(\rho \cdot Cp) \quad (5)$$

where λ is the thermal conductivity, Cp is the specific heat and ρ the oven dry density. The two heavyweight concretes have a lower thermal diffusivity than the normal concrete, mostly explained by their lower thermal conductivity and higher density. The EAF diffusivity value of 0.89 mm^2/s is in agreement with results found by Adegoloye et al. (2015), ranging from 0.86 and 0.96 mm^2/s. Like barite concrete, EAF concrete has favourable heat insulation properties.

Figure 14 presents the evolution of thermal conductivity of EAF and BAR concretes as a function of the temperature during heating up to 600°C. Limitation in the thermal properties measures is caused by the use of nickel in the spiral of the probe. Nickel exhibits a change in its electrical properties near its Curie temperature that occurs at 358°C, around which measurements do not give physically meaningful values in the range between 350 and 400°C.

The observation of the thermal conductivity curves of the different concretes (Figure 14) as a function of temperature showed, as expected, that the thermal conductivity decreased with temperature. Phonons, quanta of atomic vibrational modes are the main heat carrier in non-metallic solids (Zinan, 1960). At high temperature, the decrease of thermal conductivity with temperature is related to phonon-phonon interaction (Minnich 2015). This decrease is also linked to the increase of pores due to decomposition of hydrates and thermal microcracking. Usually, the most conductive concretes show a higher loss of conductivity with the rise of temperature (Xing et al. 2015). EAF concrete conductivity is higher than BAR concrete conductivity at room temperature, but the conductivity of EAF concrete shows a lower loss of conductivity with temperature. Up to 300°C, the EAF concrete exhibits a lower conductivity decreasing rate, this being 0.07 $W.m^{-1}$. per 100°C, compared to values found in literature, for normal-weight concretes, ranging from 0.12 to 0.2 $W.m^{-1}$ per 100°C (Kodur 2014).

Table 6: Thermal properties of REF, BAR and EAF concretes at room temperature

Concrete	Thermal Conductivity ($W \cdot m^{-1} \cdot K^{-1}$)	Thermal diffusivity (mm^2/s)	Specific heat (kJ/(kg.K))
REF	2.05 ± 0.037	1.37 ± 0.002	0.64 ± 0.058
BAR	1.34 ± 0.003	1.10 ± 0.002	0.46 ± 0.02
EAF	1.51 ± 0.012	0.89 ± 0.002	0.63 ± 0.02

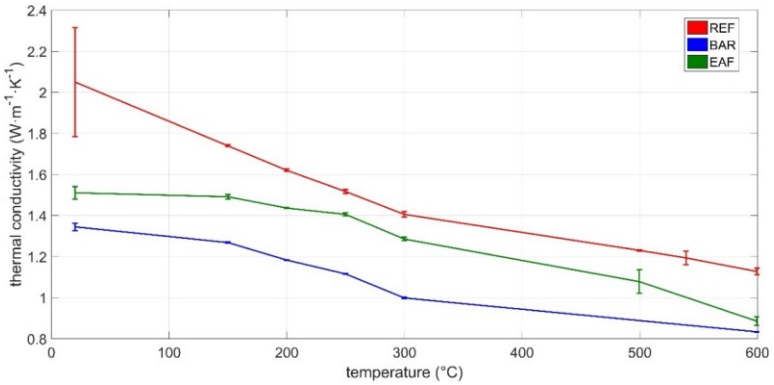

Figure 14: Thermal conductivity evolution of REF, BAR and EAF concretes with temperature during heating at 1°C/min up to 600°C.

4 Conclusion

This study aims to compare the behaviour of two different heavyweight concretes and a normal-weight concrete exposed to high temperature: a heavyweight concrete using steel industry co-products (EAF concrete), a heavyweight concrete with barite aggregates (BAR concrete) and a dolomite concrete (REF concrete) were analysed. All the concrete mixes have the same paste volume and water/cement ratio inducing an initial similarity of the cement matrix; the behaviour differences can therefore only be attributed to the nature of the aggregates.

According to the results obtained, it can be concluded that:

Barite and EAF concretes nearly have similar density, 2766 kg/m^3 and 2804 kg/m^3, respectively. Up to 300°C, the density of these two concretes remains above 2600 kg/m^3, which is the threshold defined by EN 206 for heavyweight concretes.

Concrete specimens with EAF aggregates have shown better mechanical properties compared to REF and BAR concretes. EAF concretes had the highest compressive strength at room temperature: 65 MPa vs 47 MPa and 49 MPa, compared to BAR and REF concretes respectively, and this occurs similarly at high temperature. The EAF and BAR concretes show a smaller decrease of the residual compressive strength and dynamic modulus with the temperature, while a strong degradation with the temperature was observed for the REF concrete. The best mechanical residual properties of EAF concrete is attributed to both the

strong bond between the paste and the aggregates, and the thermal behaviour of the EAF slag aggregate. SEM analysis on concretes heated at 450°C showed cracks leaving debonded aggregate grains on REF concrete, and cracks through barite aggregate grains.

The EAF concrete has a slightly higher conductivity (1.51 $W.m^{-1}.K^{-1}$) than BAR concrete (1.34 $W.m^{-1}.K^{-1}$), but a higher specific heat, so the EAF concrete thermal diffusivity is slightly lower than that of the BAR concrete. With the increase of the temperature, the thermal conductivity of the three concretes decreases and the gap between heavyweight and normal-weight concretes conductivity values decreases with the temperature.

The heating of barite aggregate at the rate of 10°C/min showed their high spalling sensitivity, which was even increased when the aggregates were in a saturated state before being heated. Barite grains were reduced into a powder form. SEM images show closed rounded micro-porosity within barite grains that might be fluid-filled considering the hydrothermal origin of barite. Heated, the barite would then be unstable under the effect of the pressure of those fluids subjected to a rise in temperature. Heated at a rate of 10°C/min, EAF aggregate showed a good thermal behaviour and TGA analysis showed a low weight loss of 0.52% at 1000°C. At a heating rate of 10°C/min up to 600°C, none of the concretes showed an explosive spalling. However, spalling aggregate at the concrete surface has been observed on EAF and BAR concretes

From the results achieved here it is possible to conclude that EAF slag can be satisfactorily used to produce heavy-weight concrete. As it is characterized by a high radiation attenuation against gamma radiation (Pomaro et al., 2019), similar and even higher than concrete made with barite aggregates, it shows promising application for radiation shielding. When it is exposed to high temperature, its residual properties are higher than that of both heavy- and normal-weight concretes. This is related to the better thermal behaviour of EAF aggregate compared to barite aggregate. However, large scale tests on real structural elements would be necessary to improve the knowledge of this material under high temperatures and fire scenarios.

5 References

Abu-Eishah, S. I., El-Dieb, A. S., & Bedir, M. S. (2012). Performance of concrete mixtures made with electric arc furnace (EAF) steel slag aggregate produced in the Arabian Gulf region. *Construction and Building Materials, 34*, 249-256.

641 Adegoloye G., Beaucour A-L, Ortola S., Noumowé A. Concretes made of EAF slag and AOD
642 slag aggregates from stainless steel process: mechanical properties and durability. *Construction*
643 *and Building Materials,* Vol. 76, 2015.

644 Alwaeli, M. (2017). Investigation of gamma radiation shielding and compressive strength
645 properties of concrete containing scale and granulated lead-zinc slag wastes. *Journal of Cleaner*
646 *Production, 166,* 157-162.

647 Arribas, I., Santamaría, A., Ruiz, E., Ortega-López, V., & Manso, J. M. (2015). Electric arc
648 furnace slag and its use in hydraulic concrete. *Construction and Building Materials*, *90,* 68-79.

649 Bangi, M. R., & Horiguchi, T. (2012). Effect of fibre type and geometry on maximum pore
650 pressures in fibre-reinforced high strength concrete at elevated temperatures. *Cement and*
651 *Concrete Research, 42(2),* 459-466.

652 Chan, S. Y., Peng, G. F., & Chan, J. K. (1996). Comparison between high strength concrete and
653 normal strength concrete subjected to high temperature. *Materials and Structures*, *29(10),* 616.

654

655 Çullu, M., & Ertaş, H. (2016). Determination of the effect of lead mine waste aggregate on
656 some concrete properties and radiation shielding. *Construction and Building Materials, 125,*
657 625-631.

658 Ducman, V., & Mladenovič, A. (2011). The potential use of steel slag in refractory concrete.
659 *Materials characterization*, *62*(7), 716-723.

660 Faleschini, F., Hofer, L., Zanini, M. A., dalla Benetta, M., & Pellegrino, C. (2017).
661 Experimental behavior of beam-column joints made with EAF concrete under cyclic loading.
662 *Engineering Structures*, 139, 81-95.

663 Faleschini, F., Santamaria, A., Zanini, M. A., San José, J. T., & Pellegrino, C. (2017). Bond
664 between steel reinforcement bars and Electric Arc Furnace slag concrete. *Materials and*
665 *Structures*, 50(3), 170.

666 Galán-Arboledas, R. J., de Diego, J. Á., Dondi, M., & Bueno, S. (2017). Energy, environmental
667 and technical assessment for the incorporation of EAF stainless steel slag in ceramic building
668 materials. *Journal of Cleaner Production*, 142, 1778-1788.

669 Gallé, C., & Sercombe, J. (2001). Permeability and pore structure evolution of silicocalcareous
670 and hematite high-strength concretes submitted to high temperatures. *Materials and Structures,*
671 *34(10),* 619.

672 Gencel, O. (2012). Effect of elevated temperatures on mechanical properties of high-strength
673 concrete containing varying proportions of hematite. *Fire and Materials, 36(3),* 217-230.

674 Glinicki, M. A., Jaskulski, R., Pichór, W., Dąbrowski, M., & Sobczak, M. (2015, September).
675 Investigation of thermal properties of shielding concretes. In *Proc. Int. Symp. Brittle Matrix*
676 *Composites, BMC-11, IPPT PAN, Warszawa*, 371-380.

677 González-Ortega, M. A., Segura, I., Cavalaro, S. H. P., Toralles-Carbonari, B., Aguado, A., &
678 Andrello, A. C. (2014). Radiological protection and mechanical properties of concretes with
679 EAF steel slags. *Construction and Building Materials, 51*, 432-438.

680 Gustavsson, M., Karawacki, E., & Gustafsson, S. E. (1994). Thermal conductivity, thermal
681 diffusivity, and specific heat of thin samples from transient measurements with hot disk sensors.
682 *Review of Scientific Instruments, 65*(12), 3856-3859.

683 Hager, I., Tracz, T., Śliwiński, J., & Krzemień, K. (2016). The influence of aggregate type on
684 the physical and mechanical properties of high-performance concrete subjected to high
685 temperature. *Fire and materials*, 40(5), 668-682.

686 Heap, M. J., Lavallée, Y., Laumann, A., Hess, K. U., Meredith, P. G., Dingwell, D. B., & Weise,
687 F. (2013). The influence of thermal-stressing (up to 1000 °C) on the physical, mechanical, and
688 chemical properties of siliceous-aggregate, high-strength concrete. *Construction and Building*
689 *Materials, 42,* 248-265.

690 Horszczaruk, E., Sikora, P., Cendrowski, K., & Mijowska, E. (2017). The effect of elevated
691 temperature on the properties of cement mortars containing nanosilica and heavyweight
692 aggregates. *Construction and Building Materials, 137*, 420-431.

693 Kaplan, M. F. (1989). Concrete radiation shielding. *John Wiley & Sons Inc, New York, 22(1)*,
694 448.

695 Kodur, V. (2014). Properties of concrete at elevated temperatures. *ISRN Civil engineering*,
696 2014, p 15.

697 Komarovskii, A.N. (1961). Shielding materials for nuclear reactors. *Pergamon Press, London*,
698 *UK*.

ha formattato: Italiano (Italia)

699 Liang, X., Wu, C., Su, Y., Chen, Z., & Li, Z. (2018). Development of ultra-high performance
700 concrete with high fire resistance. *Construction and Building Materials,* 179, 400-412.

701 Ling, T. C., & Poon, C. S. (2014). High temperatures properties of barite concrete with cathode
702 ray tube funnel glass. *Fire and Materials, 38(2),* 279-289.

703 Lo Monte, F., & Gambarova, P. G. (2014). Thermo-mechanical behavior of baritic concrete
704 exposed to high temperature. *Cement and Concrete Composites, 53,* 305-315.

705 Manso, J. M., Gonzalez, J. J., & Polanco, J. A. (2004). Electric arc furnace slag in concrete.
706 *Journal of materials in civil engineering, 16*(6), 639-645.

707 Maslehuddin, M., Naqvi, A. A., Ibrahim, M., & Kalakada, Z. (2013). Radiation shielding
708 properties of concrete with electric arc furnace slag aggregates and steel shots. *Annals of*
709 *Nuclear Energy, 53,* 192-196.

710 Maslehuddin, M., Sharif, A. M., Shameem, M., Ibrahim, M., & Barry, M. S. (2003).
711 Comparison of properties of steel slag and crushed limestone aggregate concretes. *Construction*
712 *and building materials*, 17(2), 105-112.

713 Mindeguia, J. C., Pimienta, P., Carré, H., & Borderie, C. L. (2013). Experimental analysis of
714 concrete spalling due to fire exposure. *European Journal of Environmental and Civil*
715 *Engineering, 17(6),* 453-466.

716 Minnich, A. J. (2015). Advances in the measurement and computation of thermal phonon
717 transport properties. *Journal of Physics: Condensed Matter*, 27(5), 053202

718 Mostofinejad, D., Reisi, M., & Shirani, A. (2012). Mix design effective parameters on γ ray
719 attenuation coefficient and strength of normal and heavyweight concrete. *Construction and*
720 *Building Materials, 28(1),* 224-229.

721 Netinger, I., Rukavina, M. J., & Mladenovič, A. (2013). Improvement of post-fire properties of
722 concrete with steel slag aggregate. *Procedia Engineering*, 62, 745-753.

723 Netinger, I., Varevac, D., Bjegović, D., & Morić, D. (2013). Effect of high temperature on
724 properties of steel slag aggregate concrete. *Fire safety journal*, *59*, 1-7.

725 Ortega-López, V., Fuente-Alonso, J. A., Santamaría, A., San-José, J. T., & Aragón, Á. (2018).
726 Durability studies on fiber-reinforced EAF slag concrete for pavements. *Construction and*
727 *Building Materials, 163*, 471-481.

728 Ouda, A. S. (2015). Development of high-performance heavy density concrete using different
729 aggregates for gamma-ray shielding. *Progress in Nuclear Energy, 79*, 48-55.

730 Özen, S., Şengül, C., Erenoğlu, T., Çolak, Ü., Reyhancan, I. A., & Taşdemir, M. A. (2016).
731 Properties of heavyweight concrete for structural and radiation shielding purposes. Arabian
732 Journal for Science and Engineering, 41(4), 1573-1584.

733 Papayianni, I., & Anastasiou, E. (2010). Production of high-strength concrete using high
734 volume of industrial by-products. Construction and Building Materials, 24(8), 1412-1417.

735 Pellegrino, C., Cavagnis, P., Faleschini, F., & Brunelli, K. (2013). Properties of concretes with
736 black/oxidizing electric arc furnace slag aggregate. *Cement and Concrete Composites*, *37*, 232-
737 240.

738 Pomaro, B., Gramegna, F., Cherubini, R., De Nadal, V., Salomoni V., Faleschini, F., (2019).
739 Gamma-ray shielding properties of heavyweight concrete with Electric Arc Furnace slag as
740 aggregate: An experimental and numerical study. *Construction and Building Materials, 200,*
741 *188-197.*

742 Rilem TC 129-MHT. (1995). 129-MHT: Test Methods for Mechanical Properties of Concrete
743 at High Temperatures. *Materials and Structures*, 28, 410-414.

744 Shih, P. H., Wu, Z. Z., & Chiang, H. L. (2004). Characteristics of bricks made from waste steel
745 slag. *Waste Management*, 24(10), 1043-1047.

746 Thomson, M. L., Mastalerz, M., Sinclair, A. J., & Bustin, R. M. (1992). Fluid source and
747 thermal history of an epithermal vein deposit, Owen Lake, central British Columbia: evidence
748 from bitumen and fluid inclusions. *Mineralium Deposita, 27*(3), 219-225.

749 Topcu, I. B. (2003). Properties of heavyweight concrete produced with barite. *Cement and*
750 *Concrete Research, 33(6),* 815-822.

751 Ulrich, M. R., & Bodnar, R. J. (1988). Systematics of stretching of fluid inclusions; II, Barite
752 at 1 atm confining pressure. *Economic Geology*, *83*(5), 1037-1046.

753 Valenza, K., Moritz, R., Mouttaqi, A., Fontignie, D., & Sharp, Z. (2000). Vein and karst barite
754 deposits in the western Jebilet of Morocco: fluid inclusion and isotope (S, O, Sr) evidence for
755 regional fluid mixing related to Central Atlantic rifting. *Economic Geology, 95*(3), 587-606.

756 Witte, L. P., & Backstrom, J. E. (1954, June). Properties of heavy concrete made with barite
757 aggregates. *Journal Proceedings, 51*(6), 65-88).

ha formattato: Italiano (Italia)

758 Xing, Z., Beaucour, A. L., Hebert, R., Noumowe, A., & Ledesert, B. (2015). Aggregate's
759 influence on thermophysical concrete properties at elevated temperature. *Construction and*
760 *Building Materials*, 95, 18-28.

761 Xing Z., Beaucour A-L., Noumowe A., Hebert R., Ledesert B., Influence of the nature of
762 aggregates on the behavior of concrete subjected to elevated temperature, *Cement and Concrete*
763 *Research*, Vol. 41, Issue 4, pp 392-402, Apr 2011.

764 Yermak N., Pliya P., Beaucour A-L., Simon A., Noumowe A., Influence of steel and/or
765 polypropylene fibres on the behaviour of concrete at high temperature : spalling, transfer and
766 mechanical properties, Construction and Building Materials, vol 132, 2017

767 Zhang, B. (2011). Effects of moisture evaporation (mass loss) on fracture properties of high
768 performance concrete subjected to high temperatures. *Fire Safety Journal, 46*(8), 543-549.

769 Zinan, J.M. (1960). Electrons and phonons: the theory of transport phenomena in solids: *Oxford*
770 *University Press, England*, 15(8), 469-470.